Article

Assessment of Climate Change Impact on the Annual Maximum Flood in an Urban River in Dublin, Ireland

Arunima Sarkar Basu [1], Laurence William Gill [2], Francesco Pilla [1] and Bidroha Basu [3,*]

1   School of Architecture, Planning and Environmental Policy, University College Dublin,
    D04 V1W8 Dublin, Ireland; arunima.sarkar@ucdconnect.ie (A.S.B.); francesco.pilla@ucd.ie (F.P.)
2   Civil, Structural and Environmental Engineering, Trinity College Dublin, D02 PN40 Dublin, Ireland;
    laurence.gill@tcd.ie
3   Civil, Structural and Environmental Engineering, Munster Technological University, T12 P928 Cork, Ireland
*   Correspondence: bidroha.basu@mtu.ie; Tel.: +353-21-433-5455

Abstract: Hydrological modelling to address the problem of flood risk corresponding to climate change can play an important role in water resources management. This paper describes the potential impact of climate change on an urban river catchment using a physically based hydrological model called Soil Water Assessment Tool (SWAT). The study area considered is the Dodder River basin located in the southern part of Dublin, the capital city of Ireland. Climate projections from three regional climate models and two representative concentration pathways (RPC 4.5 and RCP 8.5) were used to evaluate the impact of flooding corresponding to different climate change scenarios. Annual maximum flow (AMF) is generated by combining the bias-corrected climate projections with the calibrated and validated SWAT model to understand the projected changes in flood patterns for the year 2021–2100. The expected changes in flood quantiles were estimated using a generalised extreme value distribution. The results predicted up to 12% and 16% increase in flood quantiles corresponding to 50 years and 100 years return periods. Based on the flood quantiles, flood inundation maps were developed for the study area.

Keywords: climate change; SWAT model; quantile-based bias correction; annual maximum flood; generalised extreme value distribution; urban flood inundation maps

1. Introduction

Understanding the hydrological processes of river catchments provides essential information for effective water management [1]. The physics of the hydrological phenomena of the river catchments can be modelled using data-driven models. In these types of models, a functional relationship is developed between the output/predictand variable (streamflow data) and a set of input/predictor variables (meteorological data such as rainfall, temperature, humidity, solar radiation, and wind speeds that are known to influence the runoff generation mechanics) [2]. Some examples of data-driven models are Artificial Neural Networks (ANN) [3–5], fuzzy logic [6–8], time series analysis [9,10] and support vector machine [11–13]. Data-driven simple statistical models are easily implementable but fail to capture the physical process of the runoff generation mechanism. On the other hand, the physical-based hydrological models are more complex and take more time to develop but are found to have better accuracy in simulating runoff [2,14,15].

The Soil Water Assessment Tool (SWAT) model is a physically based model and is an effective tool used for simulating hydrological processes, soil erosion, and assessing the effects of climate change, land-use change, and water management practices in diverse environmental conditions [16–18]. The SWAT model has been used as a tool to help with the implementation of various environmental laws and policies, such as the Clean Water Act in the United States [19] or the European Water Framework Directive [20]. One of the primary functions of the SWAT model is to perform streamflow forecasting in river basins, which is

essential for effective water resources management and flood management practices [21]. Many studies have reported that most flood occurrences have been caused by extreme rainfall events [22], prolonged rainfall, or intense snowmelt [23]. Uncertainties associated with climate change are linked to changing dynamics of precipitation which range from variations in changes in the amount, intensity, and frequency of precipitation [24]. Hydro-climatic approaches, therefore, need to be used to study catchment runoff responses due to varying precipitation patterns in order to understand the magnitude, intensity, and frequency of extreme flood events [25,26].

Floods have resulted in the loss of human lives and property [27]. Between 1980 and 2016, more than one-third of the reported economic losses in the European Union occurred due to flooding [28]. Climate change has been linked with an increase in flood events in Ireland by Kiely [29], while Leahy and Kiely [30] used generalised Pareto distribution to estimate flood quantiles corresponding to 10-year and 30-year return periods based on historical flood data obtained for pre-1975 (pre climate change) and post-1975 (post climate change) and compared the quantiles obtained pre and post climate change period. The results indicated that considerably greater land areas are at severe risk of frequent floods when compared with pre climate change period. Fernando et al. [31] considered global rainfall and landcover database to simulate runoff at major river basins across the world in areas where real-world data are scarce and stated that the global database could be used for the development of flood risk management in data-scarce regions.

The impact of climate change can be assessed in many ways. Some common approaches include historical trend analysis, sensitivity analysis, and climate modelling [32,33]. The best way to model the mean future climate, its variability, and extremes that occur at the Earth's surface is with the use of global climate models (GCMs) [34]. GCMs are three-dimensional mathematical models based on principles of fluid dynamics, thermodynamics, as well as radiative heat transfer [35,36]. The climate system projections of GCMs are a combination of various components such as an atmospheric model for wind speeds, temperature, oceanic variables, water circulation, ice cover, soil and vegetation, heat and moisture transfer in the atmosphere, etc. [37,38]. GCMs can also simulate some of the important patterns of climate variability for time scales ranging from seasonal to annual to decadal, such as the monsoons, seasonal shifts of temperatures, etc. [39].

However, one major drawback of the GCM modelling approach is that it lacks the precision to project weather and climate variables (such as rainfall) at a local catchment scale since the GCMs are available at a much coarser spatial scale [40]. This results in a bias of variables produced by GCM. Thus, regional climate models (RCMs) have been developed to bridge the gap between global and local scale parameters [41]. The advantage of using RCMs over GCMs is that for the representation of small-scale processes, a more realistic representation can be achieved [42]. Thus, to equate the difference and bridge the gap between the climate models, techniques such as downscaling methods have been introduced [43,44]. Downscaling techniques use high-resolution dynamical or statistical methods for simulating weather and climatic variables at finer spatial resolutions [45]. The two most popular methods of downscaling are dynamical downscaling and statistical downscaling [46]. Dynamical downscaling uses high-resolution RCMs to provide simulated climate outputs at finer resolutions [47]. Dynamical downscaling has more potential for capturing nonlinear effects between many climate variables while ensuring internal consistency with regard to physical parameters [48]. This helps in processing a more realistic projection of future climatic variables [49]. However, the main drawbacks of dynamical downscaling models are their computational cost and the lack of provision of information at the catchment scale [50,51]. The skill of an RCM is dependent on biases present in the driving GCM and regional forces such as orography, land–sea contrast, and vegetation cover [38]. Alternatively, statistical downscaling develops an empirical relationship between the GCM variables (predictors) and hydrologic variables (predictands). In statistical downscaling, the accuracy of the estimates depends on the quality of data of the observations and the selected climate variables used for model performance [42]. Statistical

downscaling methods require observed values of atmospheric predictors and observed station variables [52]. The downscaling approach can be used to obtain future projections of several meteorological variables that influence flow generation mechanisms at a catchment scale [53]. Annual maximum flows (AMFs) can be derived as time series to understand the dominant flood generating factors controlling the catchment dynamics [54]. This study develops a SWAT model based on historical hydrological and meteorological data for the Dodder River catchment in order to simulate runoff corresponding to different climate change scenarios. The Dodder River is one of the most important rivers in the Dublin area. The river originates in the Dublin Mountains and meets River Liffey in the city centre of Dublin. Observations indicate that the river has overflowed its banks on numerous occasions, with the majority of those flooding occurring because of rainstorms [55]. The simulated runoff was used to extract annual maximum flow for the future, and the flood quantiles were estimated, which were then compared to flood quantiles based upon historical data. The objective of this study is to quantify the expected changes in annual maximum flow and the associated flood inundation maps in the Dodder River basin located in an urban area by considering different climate change scenarios. This information is valuable in performing risk and vulnerability assessments of flooding in an urban area in a climate change context.

2. Materials and Methods

This study uses the Soil Water Assessment Tool (SWAT) model to simulate the streamflow/runoff at a catchment outlet. The SWAT model requires a set of catchment-related and weather-related meteorological information. Historical weather data have been used to calibrate and validate the SWAT model. Subsequently, future projections of the meteorological variables corresponding to different climate change scenarios are used as an input to the validated SWAT model to simulate runoff projections. Quantile based bias correction has been applied to the future projected runoff simulations. Since this study focuses on flood analysis, the annual maximum flow (AMF) has been extracted from the bias-corrected daily runoff projections. Following this, a generalised extreme value (GEV) distribution has been fitted to the AMF data to estimate the design quantile flood corresponding to different return periods. Subsequently, flood inundation maps have been developed based on the Hydrological Engineering Centre—River Analysis System (HEC-RAS) model by using the estimated design flood quantiles obtained for different return periods.

2.1. Soil Water Assessment Tool (SWAT) Model

The SWAT model was developed by the United States Department of Agriculture for simulating water transport at a watershed/catchment/basin outlet. The model can simulate the river discharge at a daily/subdaily time scale [56,57] and requires information on the elevation, land cover, and soil attributes from the catchment, along with the meteorological variables in the region. The steps involved in the model are described below and shown in a flowchart in Figure 1.

A digital elevation model (DEM) is the primary data used by the model to delineate the catchment/watershed and develop the stream network. The DEM is also used to estimate the slope of the entire catchment. Once the watershed and the river network were formed using SWAT based on the DEM data, the SWAT model considered the land cover and the soil maps for the catchment. By integrating the land cover, soil, and the slope of the catchment, the river watershed was divided into several sub-basins, which were then further subdivided into hydrological response units (HRUs) using SWAT. The HRUs were the smallest scale sub-basins that consisted of homogeneous land cover, management (slope), and soil characteristics. The SWAT models simulated the flow from each HRUs using the following water balance equation:

$$SW_t = SW_0 + \sum_{i=1}^{n} \left(R_{day} - Q_{sur} - E_a - W_{seep} - Q_{gw} \right)_i \tag{1}$$

where t is the time (days), SW_t is final soil water content (mm), SW_0 is initial soil water content (mm), R_{day} is rainfall on i-th day (mm), Q_{sur} is surface runoff on i-th day (mm), E_a is evapotranspiration on i-th day (mm), W_{seep} is water percolating to the vadose zone on i-th day (mm), and Q_{gw} is return flow on i-th day (mm) [58], and n is the total number of days. To estimate the surface runoff in the water balance equation, the SCS curve number approach has been used in the SWAT model. Evapotranspiration is estimated based on the Penman–Monteith Equation [59], which requires values of mean temperature, wind speed, relative humidity, and solar radiation on a daily scale. In order to simulate runoff at the river basin outlet, five meteorological/weather variables, namely rainfall, temperature, relative humidity, wind speed, and solar radiation, were needed. Rainfall is one of the primary inputs to the water balance equation (Equation (1)), whereas the other four meteorological variables are used to estimate evapotranspiration using the Penman–Monteith method. The SWAT model combines the watershed-related data and the meteorological data and simulates surface and subsurface runoff at the basin outlet, as well as the groundwater recharge for the river basin.
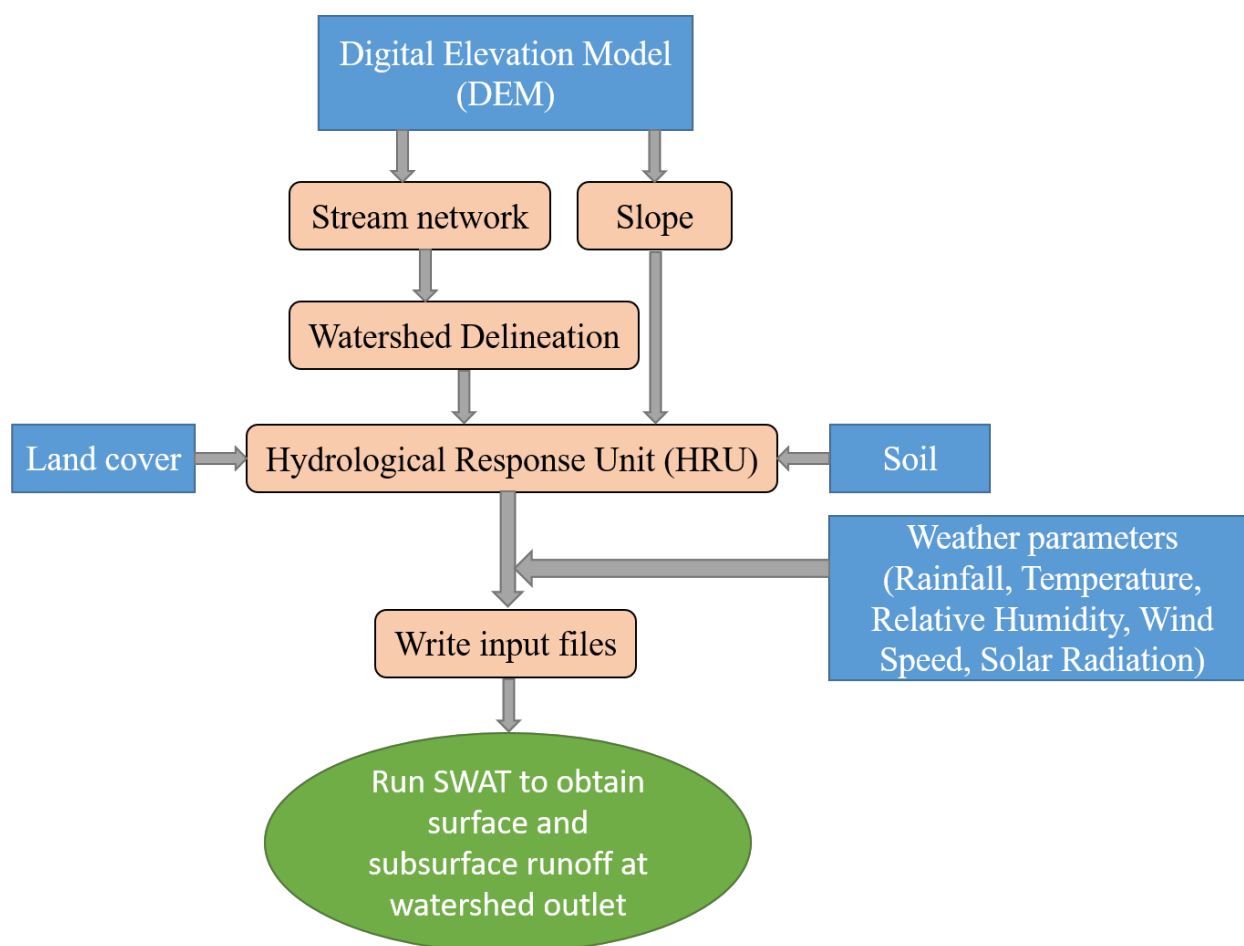
Figure 1. Flowchart of the SWAT model.

It should be noted that the SWAT model was primarily developed to simulate catchment runoff at river basins across the United States [60]. For areas located outside the United States, the SWAT model parameters need to be recalibrated. The SWAT model has more than 1100 parameters (Abbaspour); however, a literature review [61] revealed that calibration of only a limited portion of those parameters is sufficient to obtain a realistic SWAT model for a river basin.

Calibration of the model parameters can be performed by using different algorithms, such as sequential uncertainty fitting (SUFI), particle swarm optimization (PSO), gener-

alised likelihood uncertainty estimation (GLUE), parameter solution (ParaSol), and Markov chain Monte Carlo (MCMC). Each of those algorithms is available for calibration in the SWAT Calibration and Uncertainty Programs (SWAT-CUP) software developed by Abbaspour et al. [62]. This study considered SUFI version 2 (SUFI-2) available in SWAT-CUP to calibrate the important parameters of the SWAT model. The algorithm accounts for all sources of uncertainty present in the catchment-related variables and meteorological data (rainfall, temperature, relative humidity, wind speed and solar radiation), the conceptual SWAT model and its selective parameters. The degree to which the uncertainty for each variable is accounted for depends on the predictive uncertainty of the measured data. Details on the algorithm can be found in Abbaspour [63].

Once the model parameters have been calibrated, the SWAT model can be used to simulate surface runoff at the basin outlet for the historical period. The simulated runoff can be compared to the observed discharge at the location, and the difference between observed streamflow discharge and the SWAT simulated runoff can be quantified in terms of several performance measures such as Pearson correlation coefficient (CORR), Nash–Sutcliffe Efficiency (NSE), and Kling–Gupta Efficiency (KGE) as follows:

(a)   Pearson correlation coefficient (*CORR*):

$$CORR = \frac{T \sum_{t=1}^{T} \hat{y}(t) \times y(t) - \left[\sum_{t=1}^{T} \hat{y}(t)\right] \times \left[\sum_{t=1}^{T} y(t)\right]}{\sqrt{\left[T \sum_{t=1}^{T} (\hat{y}(t))^2 - (\sum_{t=1}^{T} \hat{y}(t))^2\right] \times \left[T \sum_{t=1}^{T} (y(t))^2 - (\sum_{t=1}^{T} y(t))^2\right]}} \tag{2}$$

where $y(t)$ is the observed runoff/streamflow at time t, $\hat{y}(t)$ is the SWAT model predicted runoff at time t, T is the number of data points (daily/annual maximum), and $\bar{y} = \sum_{t=1}^{T} y(t)/T$ is the mean observed flow.

(b)   Nash–Sutcliffe Efficiency (*NSE*):

$$NSE = 1 - \frac{\sum_{t=1}^{T} [\hat{y}(t) - y(t)]^2}{\sum_{t=1}^{T} [y(t) - \bar{y}]^2} \tag{3}$$

(c)   Kling–Gupta Efficiency (*KGE*):

$$KGE = 1 - \sqrt{(CORR - 1)^2 + (a - 1)^2 + (b - 1)^2} \tag{4}$$

where *CORR* is the Pearson correlation coefficient, $a = \sqrt{\frac{T \sum_{t=1}^{T} (\hat{y}(t))^2 - (\sum_{t=1}^{T} \hat{y}(t))^2}{T \sum_{t=1}^{T} (y(t))^2 - (\sum_{t=1}^{T} y(t))^2}}$, and $b = \sqrt{\frac{\sum_{t=1}^{T} \hat{y}(t)}{\sum_{t=1}^{T} y(t)}}$.

The value of NSE and KGE ranges from $(-\infty, 1]$, while CORR ranges from $[-1, 1]$. All of the performance measure values tend toward unity as model predictions become closer to the observed values.

Once the model parameters are calibrated, and the model is validated by comparing the simulated runoff with the observed streamflow discharge, the SWAT model can be used to simulate future runoff by using future projections of each of the five meteorological variables. The future projections of those variables can be obtained in a gridded format from regional climate models (RCMs) or general circulation models (GCMs). However, it should be noted that the RCM/GCM simulations induce bias in the simulated runoff [64]; hence the projected runoff needs to be bias-corrected. This study considers the quantile-based bias correction approach.

2.2. Quantile-Based Bias Correction

The quantile-based bias correction approach develops a statistical relationship/transfer function between the model outputs and the observed data based on the historical stream-flow data. Subsequently, the developed transfer function is used on the future projected runoff simulations to perform bias correction. This study considers the quantile-based mapping method as the transfer function. The bias-adjusted future runoff $Q_{fut,sum-adj.}$ can be estimated as,

$$Q_{fut,sum-adj.} = Q_{fut,sim} + F^{-1}_{hist,obs}\left(F_{fut,sim}\left(Q_{fut,sim}\right)\right) - F^{-1}_{hist,sim}\left(F_{fut,sim}\left(Q_{fut,sim}\right)\right) \quad (5)$$

where $Q_{fut,sim}$ is the SWAT model simulated runoff in the future, $F_{fut,sim}(\cdot)$ is the cumulative distribution function (CDF) of the future simulated runoff, $F^{-1}_{hist,obs}$ is the inverse CDF obtained based on the observed historical streamflow, and $F^{-1}_{hist,sim}$ is the inverse CDF developed using the simulated runoff obtained from the SWAT model in the historical time period. Details of the quantile-based bias correction approach can be found in Li et al. [65].

The distribution function for the daily runoff/streamflow can be obtained by fitting a chosen distribution or using an empirical distribution. In this study, empirical CDF has been used based on the Weibull plotting position formula, which is a commonly used approach to develop empirical CDF for daily streamflow [66]. The Weibull plotting position has been found to have unbiased exceedance probabilities for all distributions.

Once the bias-corrected runoff simulations for the future were obtained corresponding to a chosen climate change scenario, the annual maximum flow (AMF) can be extracted as the maximum value of the runoff for a chosen year. As per extreme value theory [67], the AMF time series follow an extreme value distribution. In this study, the AMF time series is considered to follow a generalised extreme value (GEV) distribution.

2.3. Generalised Extreme Value Distribution

The GEV distribution can be fitted to the AMF data in order to estimate the design flood quantiles corresponding to different nonexceedance probabilities F or return periods T. The estimated quantile value can be considered as the expected maximum flood at the outlet of the chosen catchment in the upcoming T years. This value can further be used to identify the flooded area downstream to the catchment outlet by developing flood inundation maps.

The GEV distribution is a 3-parameter distribution given by

$$F(x) = exp\left\{-\left[1 - \frac{k}{\alpha}(x - \xi)\right]^{\frac{1}{k}}\right\} \quad (6)$$

where ξ, α, and k are, respectively, the location, scale, and shape parameters of the GEV distribution. The distribution parameters can be estimated as,

$$k = \begin{cases} 0.2858221 - 0.357983CS + 0.116659CS^2 - 0.022725CS^3 + 0.002604CS^4 - 0.000161CS^5 - 0:000004CS^6; \ k < 0 \ (1.14 < CS < 10) \\ 0.277648 - 0.322016CS + 0.060278CS^2 + 0.016759CS^3 - 0.005873CS^4 - 0.00244CS^5 - 0.00005CS^6; \ k > 0 \ (0 < CS < 1.14) \\ -0.50405 - 0.00861CS + 0.015497CS^2 + 0.005613CS^3 + 0.00087CS^4 + 0.000065CS^5; \ k < 0 \ (-10 < CS < 0) \end{cases} \quad (7)$$

$$\alpha = \sqrt{\sigma^2 k^2 / \left[\Gamma(1 + 2k) - \Gamma^2(1 + k)\right]} \quad (8)$$

$$\xi = \mu - \frac{\alpha}{k}[1 - \Gamma(1 + k)] \quad (9)$$

where CS is the coefficient of skewness, σ^2 is the variance, and μ is the mean of the annual maximum flow data. Once the parameters of the GEV distribution were obtained, the

flood quantile corresponding to a different return period $T = 1/(1 - F)$ (nonexceedance probability F) can be estimated as,

$$x(F) = \begin{cases} \xi + \frac{\alpha}{k}\left[1 - (-lnF)^k\right], & if \ k \neq 0 \\ \xi - \alpha[ln(-lnF)], & if \ k = 0 \end{cases} \tag{10}$$

2.4. Hydrological Engineering Centre—River Analysis System (HEC-RAS) Model

HEC-RAS performs analysis of flow dynamics in natural rivers and channels based on hydraulic equations. The developed model can be one-dimensional (1D) as well as two or three-dimensional (2D or 3D) and can perform both steady and unsteady analyses [68,69]. The model can be used for channel flow analysis, as well as the development of floodplain maps or flood inundation maps. Horritt and Bates [70] used both 1D and 2D HEC-RAS models to develop flood inundation maps at river Severn, UK and noted that the developed maps are not significantly different. Alho and Aaltonen [71] compared the performance of 1D and 2D HEC-RAS models in the development of floodplain maps at Jökulsá á Fjöllum river, Iceland and reported that both the models create comparable results. On the other hand, Cook and Merwade [72] noted that the 1D model slightly underpredicts the inundated area when compared with the 2D counterpart, as the 1D model does not consider the flow volume information while creating floodplain maps. Costabile et al. [73] reported that the performance of both 1D and 2D HEC-RAS models in delineating flood inundation maps depends on the available topographic and river bathymetry information and the performance of those models improves significantly with accurate LiDAR/DEM data. This study develops the steady 1D HEC-RAS model to create flood inundation maps corresponding to quantiles obtained for different return periods using the following hydraulic energy equation [74]:

$$Z_2 + Y_2 + \frac{a_2 V_2^2}{2g} = Z_1 + Y_1 + \frac{a_1 V_1^2}{2g} + h_e \tag{11}$$

where Z_1 and Z_2 are the elevation of main channel inverts and locations 1 and 2 respectively, Y_1 and Y_2 are depth of water at cross-sections 1 and 2, V_1 and V_2 are the average velocities, a_1 and a_2 are velocity weighting coefficients, g is the gravitational acceleration, and h_e is the energy head loss given as,

$$h_e = L\overline{S_f} + C\left|\frac{a_2 V_2^2}{2g} - \frac{a_1 V_1^2}{2g}\right| \tag{12}$$

where L is discharge weighted reach length, $\overline{S_f}$ is friction slope between sections 1 and 2, and C is contraction loss coefficient.

3. Catchment Description and Input Data

The study was performed in the Dodder River basin (Figure 2), located in the southern part of Dublin, the capital of Ireland. The river Dodder is one of the most important rivers in the Dublin area and originates in the Dublin Mountains (on Kippure) and meets River Liffey in the city centre at Ringsend. The river is approximately 27 km long, and the overall catchment area is around 113 square km. Due to high slopes in the catchment area, the upper and middle sections of the river are highly susceptible to flooding during periods of extreme rainfall events. Recent flood events indicate that the river can exhibit a maximum flow of up to 70 m^3/s. As the size of the river basin is small with steep slopes, it usually only takes 2–3 h for the water to flow from the upstream mountains to downstream in the city, which can create flash flooding in the area. Twenty-three years of daily discharge data were obtained at Waldron bridge river gauge from 3 January 1986 till 31 December 2019 from the Irish Environmental Protection Agency HydroNet database (https://www.epa.ie/hydronet/#09010, accessed on 1 March 2022), as shown in Figure 3a.

Since the objective of the present study is flood modelling, annual maximum flow (AMF) was extracted from the daily streamflow discharge data and is shown in Figure 3b. It should be noted that the majority of the streamflow data was missing from 1987 to 1992. Screening of the daily discharge data revealed that more than 36% of data were missing for the period 1986–1995, while the percentage of missing data reduced to 3.27% for the period 1996–2019. Hence, data ranging from 1 January 1996 to 31 December 2019 were used for further analysis in this study.

In the Dodder River basin, three DEM data sources are available: the Shuttle Radar Topographic Mission (SRTM) DEM with 90 m resolution (http://srtm.csi.cgiar.org/, accessed on 1 March 2022), the Advanced Spaceborne Thermal Emission and Reflection Radiometer (ASTER) DEM with 30 m resolution (https://ssl.jspacesystems.or.jp/ersdac/GDEM/E/, accessed on 1 March 2022), and the EU DEM with 25 m resolution (https://www.eea. europa.eu/data-and-maps/data/copernicus-land-monitoring-service-eu-dem, accessed on 1 March 2022). The DEM is one of the most important data needed for the SWAT model as it is used to delineate the catchment boundary, develop the stream network in the catchment, and estimate the slope of the catchment. A fine resolution DEM can delineate the catchment and generate the stream network with considerable accuracy. In this study, the EU-DEM has been used for SWAT modelling. The EU-DEM was generated for 39 countries across Europe by DHI GRAS Geocenter Denmark [75] as a hybrid DEM based on STRM DEM, ASTER DEM, and publicly available topographic maps. It needs to be noted that even though, for the majority of the catchments, the EU-DEM can be considered to be accurate enough, the elevation values at certain pixels can be erroneous because of the presence of sudden changes in elevations at a local scale, which can lead to a generation of discontinuous river networks in the river basin using the SWAT model. One option is to perform a filling of the EU-DEM before using it for modelling. The filled EU-DEM for the Dodder River basin is shown in Figure 4a.

The land cover map was obtained from the CORINE 2018 land cover map, available for Europe (https://land.copernicus.eu/pan-european/corine-land-cover/clc2018, accessed on 1 March 2022). The CORINE land cover map has a total of 44 land cover classes, from which 13 classes are present in the study area. The land cover classes do not exactly match with the land cover classes defined in the SWAT database, and hence the CORINE land cover was reclassified to match them with the SWAT database. (see Table S1 in the Supplementary Materials). The reclassified land cover map for the Dodder River basin is shown in Figure 4b.

Soil maps for Ireland were obtained from the General Soil Map of Ireland, available at http://gis.teagasc.ie/soils/downloads.php, accessed on 1 March 2022. Similar to land cover classes, the soil classes also needed to be reclassified for the SWAT model. The reclassified soil map is shown in Figure 4c, and details on the soil categories are provided in Basu [76]. The description of soil-related parameters for each soil category can be found in Cordeiro et al. [77]. The newly developed geodatabase (SWAT2012.mdb), the lookup table for landcover (lulc_classes.txt), and the lookup table for soil (soillookup.txt), along with the filled DEM (DEM_IRL_ITM.tif), landcover map (LULC2018_IRL_ITM.tif) and soil map (SOIL_IRL_ITM.tif) for Ireland is provided in the following link https://doi.org/10.5 281/zenodo.4767926, accessed on 1 March 2022 [78] as an open-source data for public use, while the detailed description of the data is provided in Basu [76].

In general, the performance of the SWAT model is better in situations where multiple point-source meteorological data are available for analysis. Figure 5 provides the locations of the rainfall, temperature, and weather stations that measure relative humidity (RH), wind speed (WS), and solar radiation (SR), with specific details of the Met Eireann stations given in Table S2 in the Supplementary Materials. It can be noted from Figure 5 that only three rain gauges (S1923, S5623, S6623) are located inside the Dodder River basin, whereas no Met Eireann stations are present inside the basin measuring temperature, relative humidity, wind speed, or solar radiation. Furthermore, data from station S1923 are unavailable from October 2014.
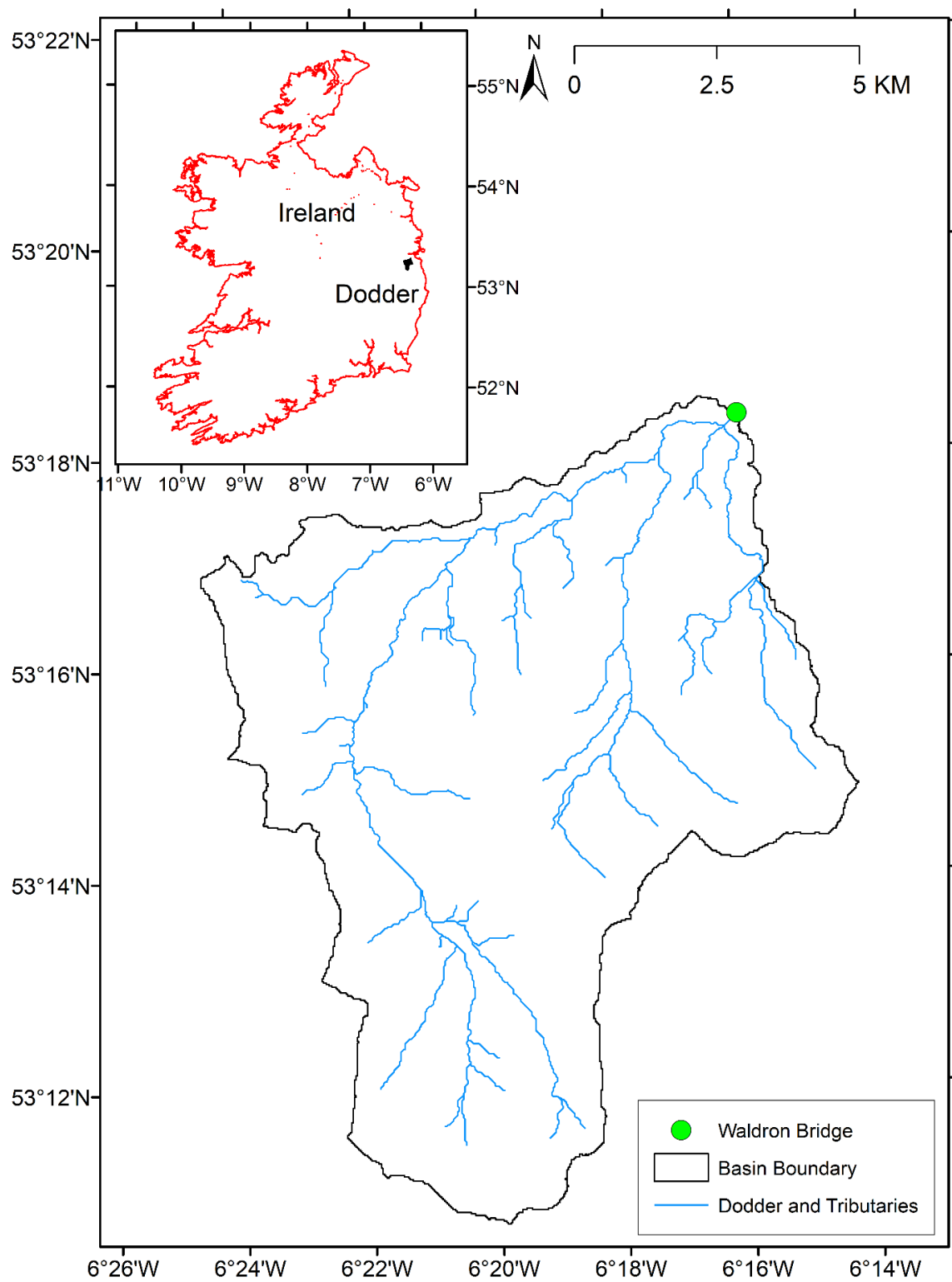
**Figure 2.** Location of Dodder River basin and the river gauge at Waldron bridge.

(**a**)

(**b**)
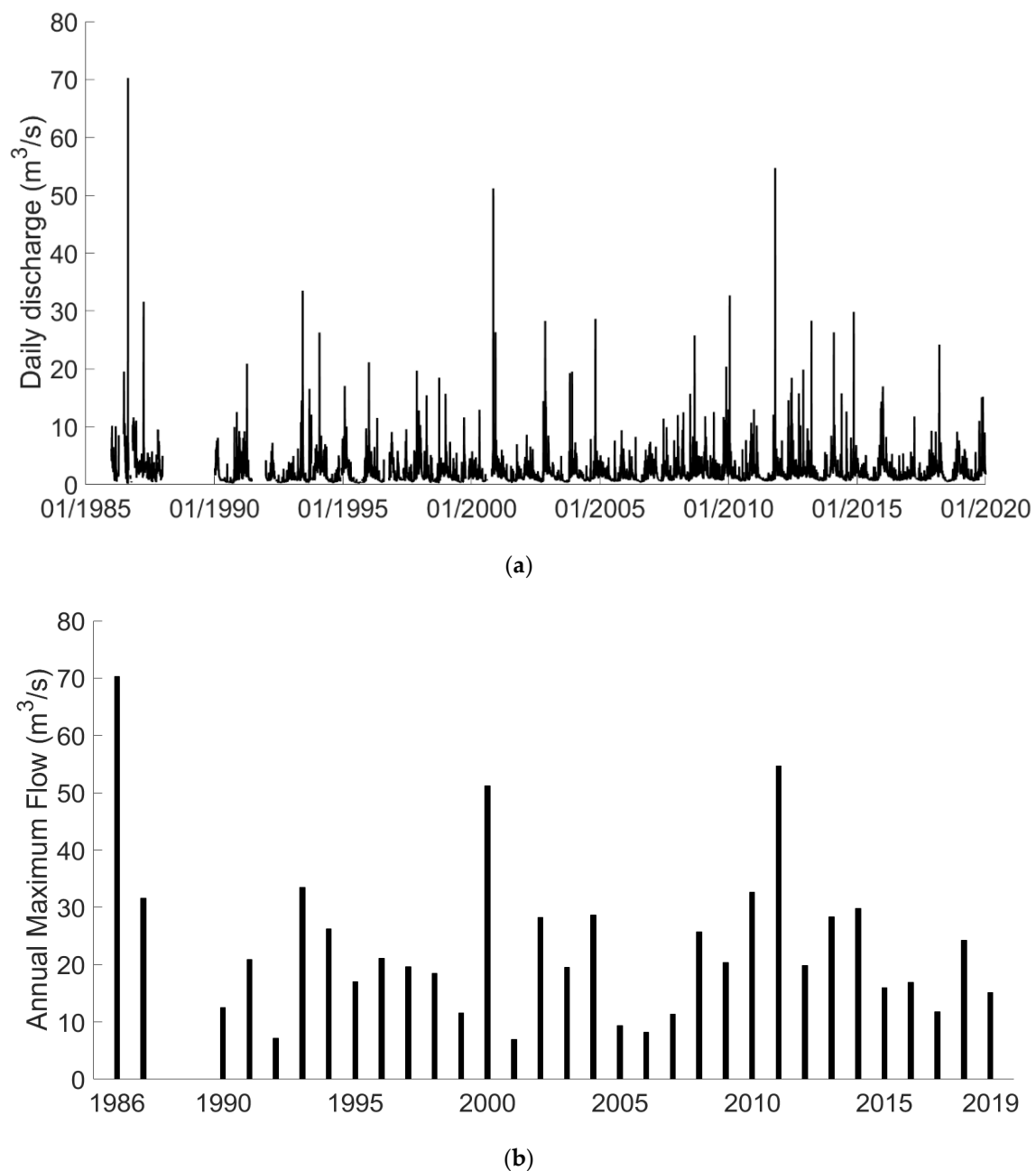
Figure 3. Time series plot of (**a**) daily discharge and (**b**) annual maximum flow observed at Waldron bridge river gauge.

Hence, because of the scarcity of on-site weather data for all meteorological variables except rainfall, only rainfall data from observed rain gauges were considered for the development of the SWAT model using three rain gauges, S3723, S5623, and S6623. The other four meteorological variables, temperature, relative humidity, wind speed, and solar radiation, required for the development of the SWAT model were obtained at a gridded scale from COPERNICUS E-OBS and ERA-5 Land database. In order to ensure the gridded weather variables reflects reality, the rainfall data obtained from E-OBS and rain gauge station S6623 were compared in terms of correlation and bias. The estimated measures were found to be 0.92, and the bias was found to be 0.74 mm, indicating that the E-OBS data matched closely with the observed rainfall. The observed rainfall is measured at a given location, whereas the gridded rainfall represents the average rainfall that occurred over the entire grid, and hence it should not be expected that both time series data perfectly match.
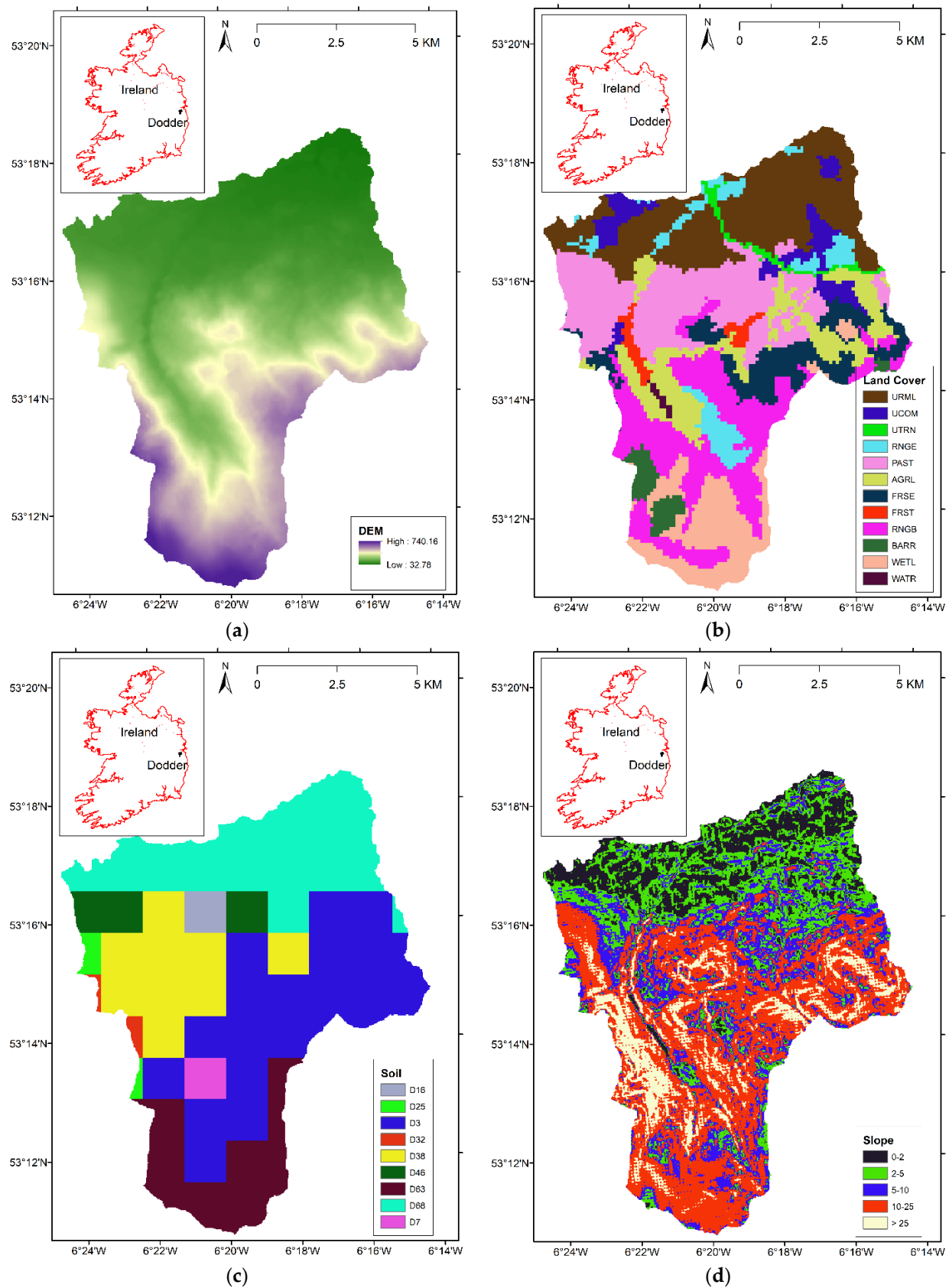
Figure 4. (**a**) EU Digital Elevation Model, (**b**) CORINE land cover, (**c**) Soil, and (**d**) Slope map for the Dodder River basin study area.
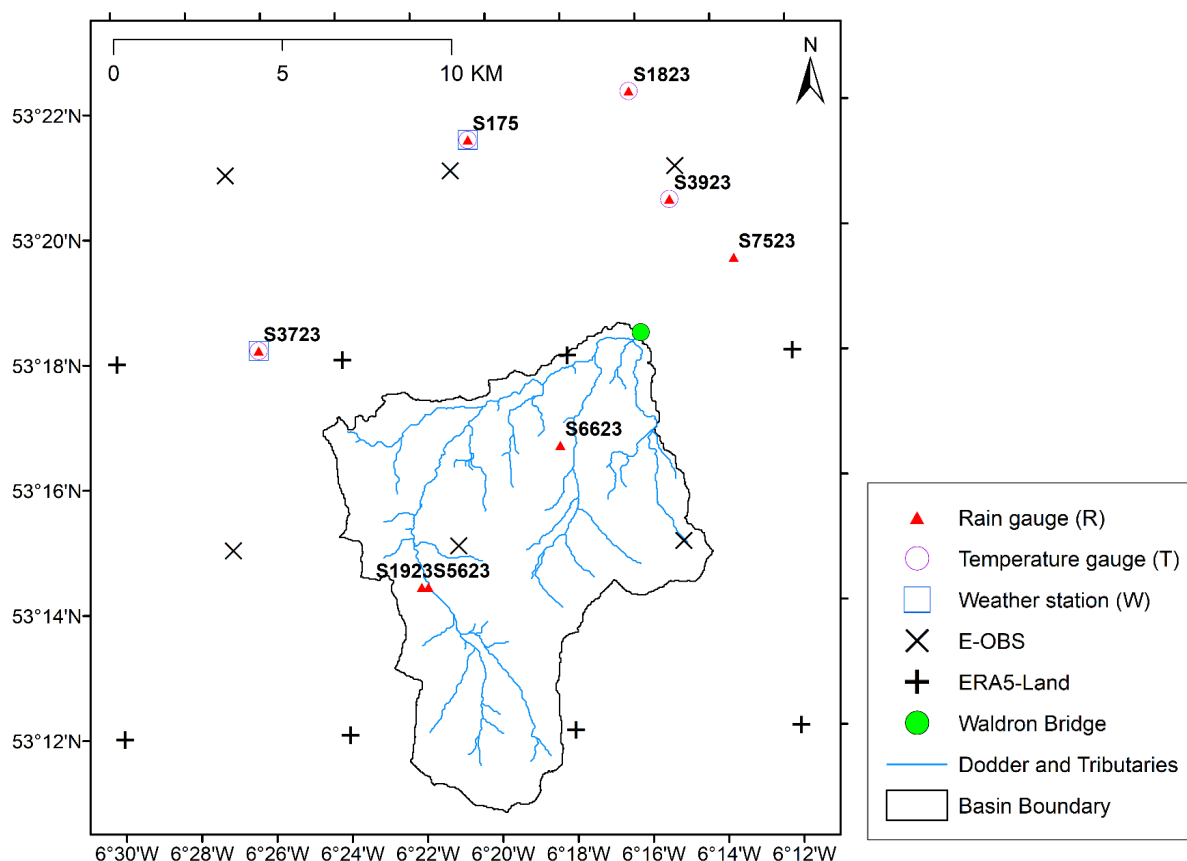
Figure 5. Locations of Met Eireann (i) rain gauges (R), (ii) temperature gauges (T), (iii) weather stations (W) measuring RH, WS and SR, (iv) E-OBS Grids for temperature, relative humidity and solar radiation, and (v) ERA5-Land Grids for wind speed along with Dodder River basin boundary.

The COPERNICUS E-OBS dataset is generated based on a network of station data observations from European National Meteorological and Hydrological Services and other European database centres. The dataset covers the majority of Europe and provides rainfall, maximum and minimum temperature, relative humidity, and shortwave solar radiation at 0.1° grid spacing on a daily time scale from the year 1950 till the present time. The data have been obtained from the following link: https://cds.climate.copernicus.eu/cdsapp#!/dataset/insitu-gridded-observations-europe?tab=form, accessed on 1 March 2022. Wind speed is not available in this dataset, so the ERA5-Land data from the COPERNICUS database have been used to obtain the wind speed data in this study. The ERA-5 Land data are available from the year 1981 to the present date at an hourly time scale at a 0.1° spatial interval covering the entire globe. The data are available from the link https://cds.climate.copernicus.eu/cdsapp#!/dataset/reanalysis-era5-land?tab=form, accessed on 1 March 2022. Locations of the E-OBS grids and the ERA5 grids used for this study covering the Dodder River basin are shown in Figure 5.

The future projections of the five meteorological variables can be obtained from a set of regional climate models (RCMs) corresponding to different representative concentration pathway (RCP) scenarios. In this study, three RCMs were considered to obtain future projections of the meteorological variables. The three RCMs considered in the study are the Koninklijk Nederlands Meteorologisch Instituut (KNMI) RACMO22E RCM, Swedish Meteorological and Hydrological Institute (SMHI) RCA4 RCM, and Danish Meteorological Institute (DMI) HIRHAM Version 5 RCM. The aforementioned three RCMs have been used by previous studies in Ireland to simulate future climate and were found to be effective [79]. The RCMs were developed in the framework of the European branch of the Coordinated Downscaling Experiment (CORDEX) of the World Climate Research

Programme (WCRP), referred to as EURO-CORDEX, at 0.11° spatial resolution (~12.25 km) covering the period 1981–2100.

The development of flood inundation maps requires detailed information on the river bathymetry. This study develops the bathymetry information from high-resolution Bluesky digital elevation model data available for the Dublin city at 1 m spatial resolution (https://www.bluesky-world.com/standard-height-data, accessed on 1 March 2022). A map of the DEM is shown in Figure S1 in the Supplementary Materials.

4. Results and Discussion

The catchment boundary upstream to the Waldron bridge river gauge in the Dodder River basin was delineated, and the river network was obtained using the EU-DEM based SWAT model (Figure 2). The basin area was estimated to be 92.3 km^2.

The slope of the catchment were estimated from DEM and were classified into five classes: 0–2%, 2–5%, 5–10%, 10–25%, and >25% (Figure 4d). Subsequently, the hydrological response units (HRUs) for the Dodder River basin were generated by combining the land cover, soil, and slope information. In total, 94 HRUs were created across the catchment, each with a unique combination of land cover, soil, and slope properties.

Once the HRUs are developed, the daily rainfall data obtained from Met Eireann rain gauges, maximum and minimum temperatures, relative humidity, wind speed, and solar radiation data obtained from the ERA5 database were fed into the SWAT model to simulate surface runoff for the period of 1 January 1996 to 31 December 2019. Since the river basin is located outside the United States, it was important to recalibrate the key SWAT model parameters that influence the runoff process. For this purpose, the SUFI-2 algorithm available in SWAT-CUP has been used, and four SWAT model parameters found to have a significant impact on the runoff simulation were chosen for recalibration: (i) Curve Number (CN), (ii) Baseflow recession coefficient (ALPHA_BF), (iii) Groundwater delay time (GW_DELAY), and (iv) Depth of water in a shallow aquifer (GWQMN). It needs to be noted that depending on location, size, and other catchment and weather-related characteristics of the river basin, some other SWAT parameters (such as soil evaporation compensation factor, groundwater RECAP coefficient, an available water capacity of the soil layer, overland Manning roughness, soil saturated hydraulic conductivity, average slope steepness, etc.) needed to be included in the recalibration process. Each of those four parameters was perturbed for the recalibration process, and the optimal values of those parameters were obtained. The range of recalibration and the optimal parameters are shown in Table 1.

Table 1. Range and the optimal value of chosen SWAT model parameters in SWAT-CUP simulation study.

| SWAT Parameter	Perturbation Range		Optimal Value
	Minimum	Maximum	
Curve Number (CN)	0	0.5	0.225
Baseflow recession coefficient (ALPHA_BF)	0	1	0.795
Groundwater delay time (GW_DELAY)	25	500	32.35
Depth of water in a shallow aquifer (GWQMN)	0	2	1.63

Once the chosen parameters were recalibrated, the SWAT model was rerun using the recalibrated parameters, and the daily surface runoff was re-estimated. Subsequently, the annual maximum flow (AMF) time series was extracted from the daily simulated runoff for the historical period (1996–2019) and compared to the observed AMF values obtained from the river gauge located at Waldron bridge in terms of three performance measures. The

values of those performance measures for daily runoff as well as for AMF were provided in Table 2, whereas the observed and SWAT-simulated AMF time series plot for 1996–2019 was shown in Figure 6. The performance of the SWAT model in predicting AMF is found to be better than its prediction of average flow on a daily scale. However, it needs to be noted that the objective of this study is to analyse the floods and not to simulate daily streamflow. In the case of AMF prediction, the correlation was greater than 0.9, while the NSE was 0.772 and KGE was 0.815. A comparison of the AMF time series plots showed that the SWAT model successfully predicts the high flows that occurred in the years 2000 and 2011. Overall, it can be concluded that the performance of the SWAT model in simulating/predicting AMF is acceptable, and so the model was then used to predict AMFs for the future corresponding to different climate change scenarios.

Table 2. Three performance measures Pearson correlation coefficient (CORR), Nash–Sutcliffe Efficiency (NSE) and Kling–Gupta Efficiency (KGE) at daily and annual maximum flow (AMF) time series for the period 1996–2019.

Time Series	CORR	NSE	KGE
Daily	0.776	0.548	0.713
AMF	0.905	0.772	0.815
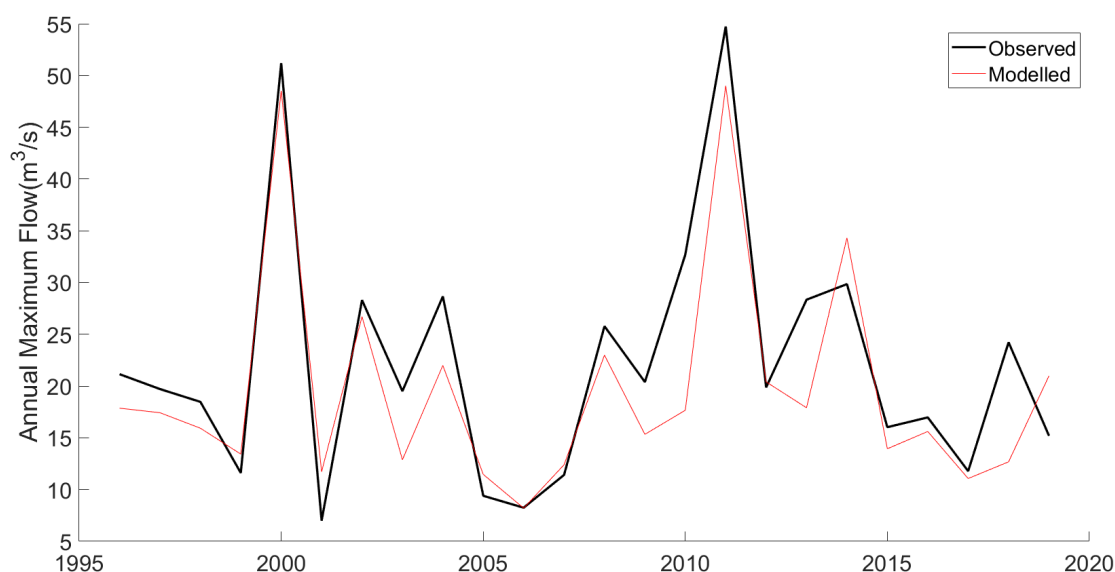
Figure 6. Comparison of annual maximum flow at Waldron bridge based on observations (OBS) and SWAT model simulations for the period 1996–2019.

This study considered three regional climate models (RCMs) and two representative concentration pathways (RCP4.5 and RCP8.5) for climate projections. The RCP4.5 is termed an intermediate scenario by the Intergovernmental Panel on Climate Change (IPCC), where the radiative forcing was assumed to be 4.5 W/m^2 in 2100. In this scenario, the greenhouse gases emissions are considered to peak around 2040, with CO_2 emissions then declining to half of the 2050 levels by 2100 [80], causing the global temperature to rise by an expected 2–3 °C by 2100. For the RCP8.5 scenario, the radiative forcing is expected to reach 8.5 W/m^2, which assumes that greenhouse gas emissions will continue to rise throughout the 21st century. Based on the projections obtained for the five meteorological variables (rainfall, temperature, relative humidity, wind speed, and solar radiation) using each of the three RCMs and the two RCP scenarios, the future projections of the flow at the Waldron bridge gauging station were obtained. The bias-corrected runoff for each scenario is provided in Figure 7. This shows that the maximum simulated AMF in the upcoming 80 years from 2021 to 2101, based on all the three models and the two RCP scenarios, is

expected to be higher than any of the observed AMFs to date over the past 24 years. The simulations based on all three RCM models also indicate that for the majority of the years, the AMF is expected to be higher for the RCP 8.5 scenario when compared with the RCP 4.5 scenario, as expected. The SMHI and DHI RCMs indicate that the AMF is expected to be low between the period 2030–2045 for both RCP scenarios but will become higher after 2060. The KNMI RCM predicts relatively high AMFs for all future years up until 2100.

(**a**)

(**b**)

(**c**)
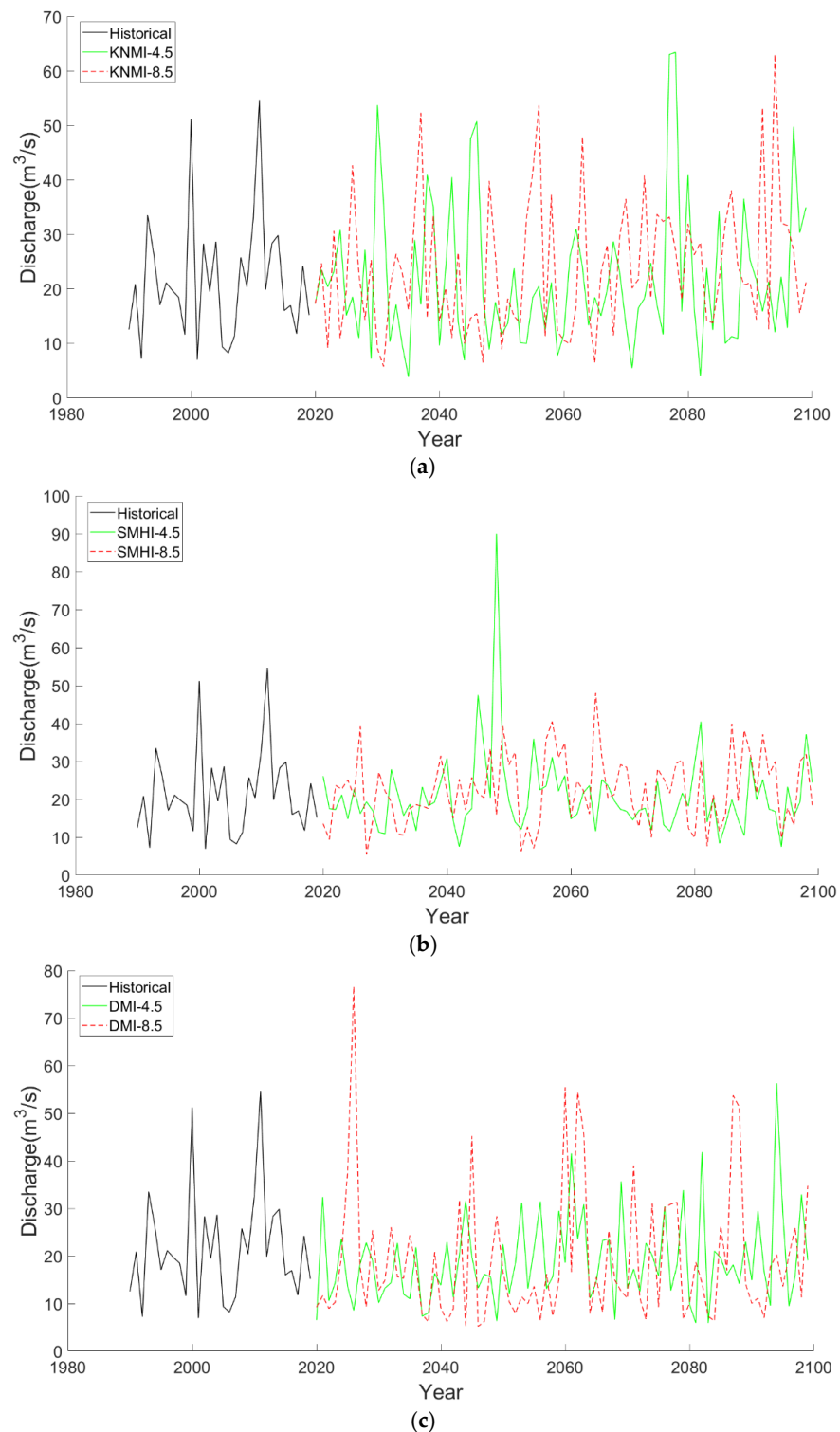
Figure 7. Projected Annual Maximum Flow plots corresponding to RCP scenarios RCP4.5 and RCP8.5 obtained from the SWAT model using (**a**) KNMI RCM, (**b**) SMHI RCM, and (**c**) DMI RCM.

The simulated AMF time series data have been used to estimate the GEV parameters for each of the RCM models and the RCP scenarios. Parameters of the fitted GEV distribution for each simulated AMF are provided in Table 3. Based on the fitted distribution, the flood quantile curve corresponding to different return periods was prepared (Figure 8). The figure indicates that KNMI-4.5, SMHI-4.5, and DMI-8.5 future scenarios produce higher flood quantiles in the future when compared with the floods observed in the past 30 years, that KNMI-8.5 predicts similar flood quantiles to the historical data, whereas SMHI-8.5 and DMI-4.5 indicate a reduction in flood quantiles in the future. For comparison purposes, quantiles corresponding to 50-, 100-, 200-, 500-, and 1000-year return periods for the historical and future periods are shown in Table 4. This shows that based on KNMI RCM 4.5, the flood quantile is expected to increase from 9–13% in the future, whilst according to the SMHI-8.5 and DMI-4.5 RCM, the flood quantile is predicted to decrease by 15–32%. The DMI-8.5 RCM predicted a maximum increase of 16.2% flood quantile corresponding to a 100-year return period, while SMHI-4.5 RCM predicted a 31.3% increase in flood quantile for the 1000-year return period.

Table 3. Parameters of the fitted GEV distribution of the Annual Maximum Flood (AMF) time series obtained from the SWAT model for the historical and future periods.

| AMF Time Series	GEV Distribution Parameters		
	Location (ξ)	Scale (α)	Shape (k)
Historical	16.534	8.535	−0.017
KNMI-4.5	15.926	9.747	−0.025
KNMI-8.5	18.491	9.983	0.043
SMHI-4.5	16.156	5.819	−0.202
SMHI-8.5	18.877	8.709	0.183
DMI-4.5	14.833	7.107	−0.013
DMI-8.5	12.625	9.651	−0.083
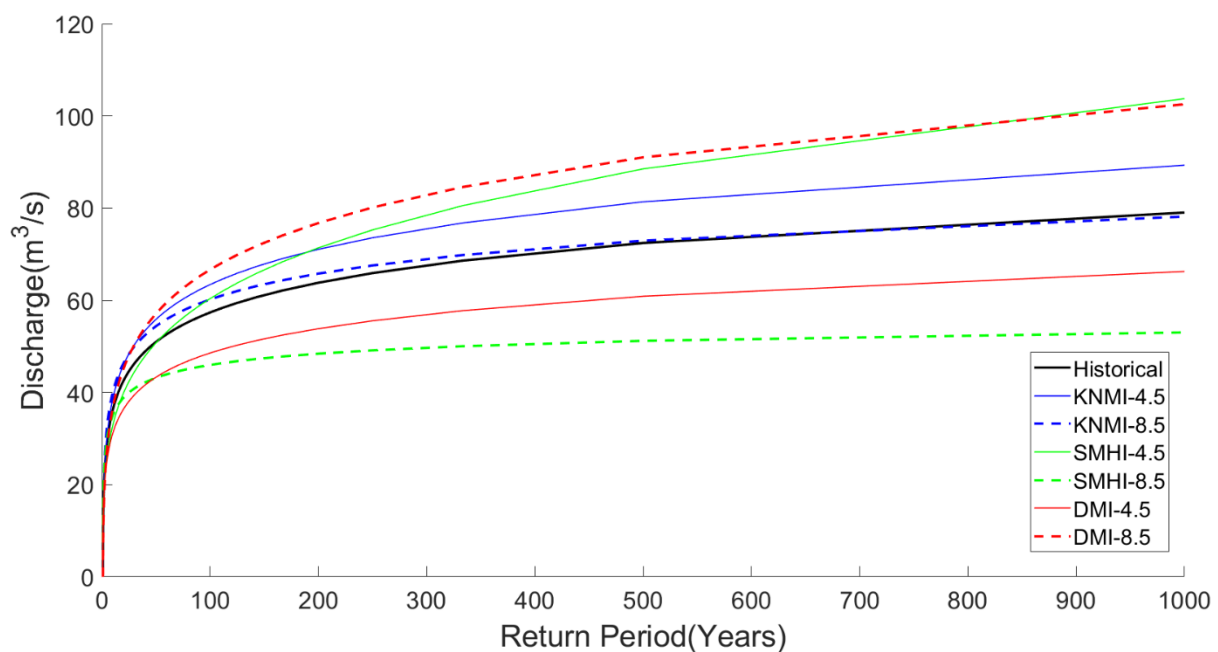
Figure 8. Quantile plot of maximum annual flows using GEV distribution for the historical and future climate change scenarios.

Table 4. Quantiles obtained using the fitted GEV distribution of the Annual Maximum Flood (AMF) time series obtained from the SWAT model for the historical and future periods. Values in parenthesis indicate increase (bold) or decrease (italics) in flood quantile with respect to historical time periods.

AMF Time Series	Return Period (Years)				
	50	**100**	**200**	**500**	**1000**
Historical	50.9	57.3	63.8	72.4	79.0
KNMI-4.5	55.8 (**9.6%**)	63.4 (**10.6%**)	71.1 (**11.4%**)	81.4 (**12.3%**)	89.3 (**13.0%**)
KNMI-8.5	54.4 (**6.7%**)	60.2 (**4.9%**)	65.8 (**3.1%**)	72.9 (**0.7%**)	78.2 (*−1.1%*)
SMHI-4.5	50.7 (*−0.4%*)	60.3 (**5.2%**)	71.4 (**11.9%**)	88.5 (**22.2%**)	103.7 (**31.3%**)
SMHI-8.5	43.2 (*−15.3%*)	46.0 (*−19.9%*)	48.4 (*−24.1%*)	51.2 (*−29.3%*)	53.0 (*−32.9%*)
DMI-4.5	43.3 (*−15.0%*)	48.5 (*−15.3%*)	53.8 (*−15.6%*)	60.9 (*−16.0%*)	66.2 (*−16.2%*)
DMI-8.5	57.1 (**12.0%**)	66.6 (**16.2%**)	76.8 (**20.3%**)	91.0 (**25.7%**)	102.5 (**29.7%**)

Based on the quantiles obtained for the historical and future period, flood inundation maps have been developed from the catchment outlet at Waldron bridge to the point where the Dodder River meets the River Liffey in Dublin city Ringsend. The river bathymetry was estimated using the Bluesky DEM, as shown in Figure 9, where the Dodder River's bank lines, flow paths, and the selected cross-sections are shown along with the elevation data.
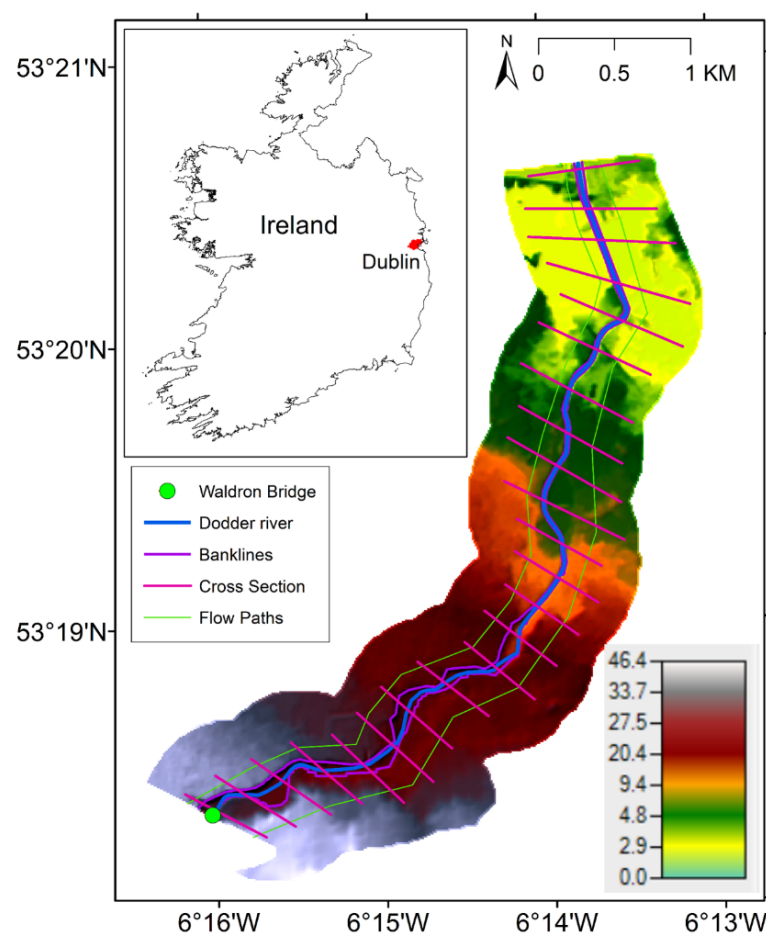
Figure 9. River bathymetry profile used to develop the HRC-RAS model.

Based on this information, the flood inundation maps were developed corresponding to five return periods: 50, 100, 200, 500, and 1000 years. For brevity, the flood inundation maps obtained based on the flood quantiles for the historical period and DMI-8.5 RCM are

shown in Figure 10, while the expected changes in the total flooded area and the maximum water depth are shown in Table 5. The results indicate a 5–13% increase in the total flooded area and a 6–19% increase in water depth of floods in the future as per the DMI-8.5 RCM compared with the historical period.
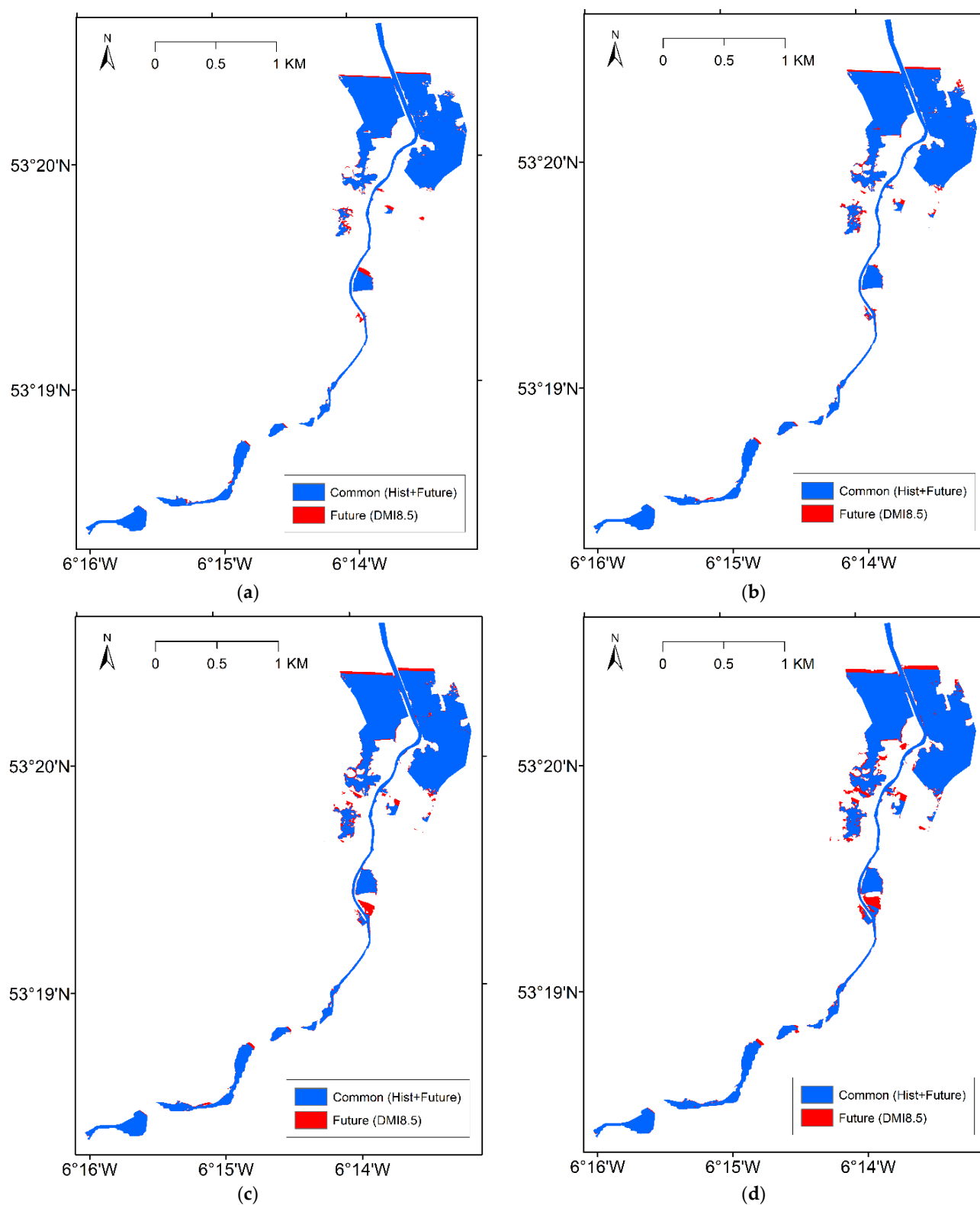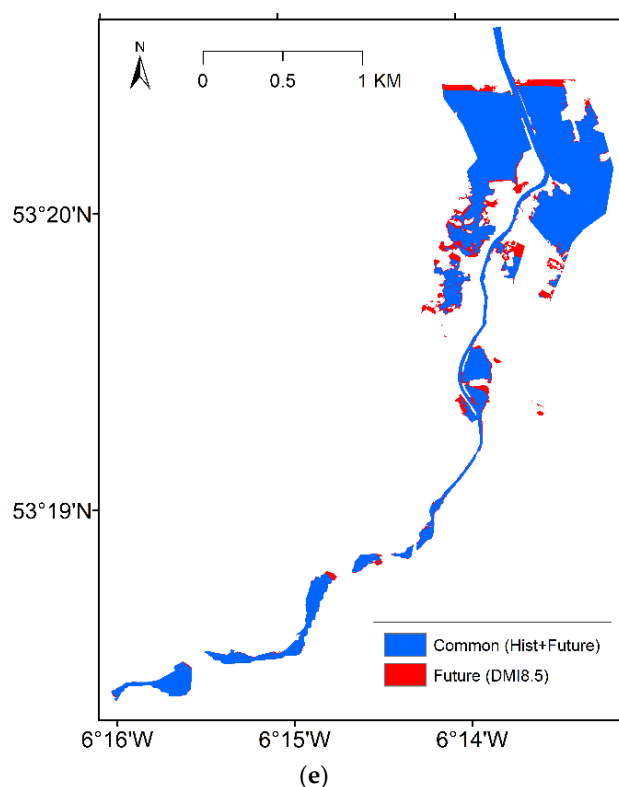

Figure 10. *Cont*.

(**e**)

Figure 10. Flood inundation maps corresponding to different return periods for the historical and future periods. (**a**) 50 years return period; (**b**) 100 years return period; (**c**) 200 years return period; (**d**) 500 years return period; (**e**) 1000 years return period.

Table 5. Total flooded area and water depths obtained from the flood inundation maps developed for the historical and future period (DMI8.5) using HEC-RAS.

Return Period (Years)	Flooded Area (km^2)				Maximum Water Depth (m)			
	Historical	Future (DMI8.5)	Difference	% Increase	Historical	Future (DMI8.5)	Difference	% Increase
50	0.766	0.804	0.038	4.98	0.570	0.609	0.038	6.73
100	0.806	0.856	0.050	6.22	0.611	0.663	0.052	8.58
200	0.842	0.910	0.068	8.07	0.648	0.715	0.067	10.36
500	0.886	0.981	0.095	10.77	0.693	0.781	0.088	12.65
1000	0.923	1.045	0.122	13.27	0.726	0.866	0.140	19.32

5. Conclusions

A Soil Water Assessment Tool (SWAT) based hydrological model has been developed for the Dodder River basin, which ends up covering the majority of the southern part of Dublin, the capital city of Ireland. As the basin is relatively small in size and its upstream catchment is located in the Wicklow mountains with steep slopes, the basin is prone to flooding. Based on historical hydrometeorological data over the past 24 years (1996–2019), the SWAT model has been calibrated and validated. The model was then used to simulate daily runoff from 2021 to 2100, and the annual maximum flow series were extracted after performing quantile-based bias correction. The future simulations were performed based on meteorological data obtained from three RCM models and two RCP scenarios. The model simulations indicate a possible increase in future flood quantile up to 16% for the 100-year return period frequency and 31% for the 1000-year return period frequency. Furthermore, the development of flood inundation maps indicates a 5–13% expected increase in the

flooded area and a 6–19% increase in water depths in the future, corresponding to return periods from 50 to 1000 years. Hence, this analysis can be utilised to create better stormwater drainage management to account for the expected increase in the percentage of floods in the future. Another point to be noted is that the runoff at the river basin outlet depends on the changes in land cover as well as weather variables [81]. In order to incorporate the potential land cover change for the future period, a land cover projection model needs to be developed by considering factors such as demography, economy, and environment. Ongoing research focuses on the development and integration of the land cover change model into the developed SWAT model by considering climate change to simulate future projected runoff at river basins across Ireland.

References

1. Hamlet, A.F.; Lettenmaier, D.P. Effects of climate change on hydrology and water resources in the Columbia river basin. *JAWRA J. Am. Water Resour. Assoc.* **1999**, *35*, 1597–1623. [CrossRef]
2. Basu, B.; Nogal, M.; O'Connor, A. New approach to multisite downscaling of precipitation by identifying different set of atmospheric predictor variables. *J. Hydrol. Eng.* **2020**, *25*, 4020013. [CrossRef]
3. Jahangir, M.H.; Reineh, S.M.M.; Abolghasemi, M. Spatial predication of flood zonation mapping in Kan River Basin, Iran, using artificial neural network algorithm. *Weather. Clim. Extrem.* **2019**, *25*, 100215. [CrossRef]
4. Tabbussum, R.; Dar, A.Q. Performance evaluation of artificial intelligence paradigms—Artificial neural net-works, fuzzy logic, and adaptive neuro-fuzzy inference system for flood prediction. *Environ. Sci. Pollut. Res.* **2021**, *28*, 25265–25282. [CrossRef] [PubMed]
5. Xie, S.; Wu, W.; Mooser, S.; Wang, Q.J.; Nathan, R.; Huang, Y. Artificial neural network based hybrid modeling approach for flood inundation modeling. *J. Hydrol.* **2021**, *592*, 125605. [CrossRef]
6. Gutenson, J.L.; Ernest, A.N.S.; Oubeidillah, A.A.; Zhu, L.; Zhang, X.; Sadeghi, S.T. Rapid flood damage pre-diction and forecasting using public domain cadastral and address point data with fuzzy logic algorithms. *JAWRA J. Am. Water Resour. Assoc.* **2018**, *54*, 104–123. [CrossRef]
7. Sahana, M.; Patel, P.P. A comparison of frequency ratio and fuzzy logic models for flood susceptibility assessment of the lower Kosi River Basin in India. *Environ. Earth Sci.* **2019**, *78*, 289. [CrossRef]

8.　Li, J. A data-driven improved fuzzy logic control optimization-simulation tool for reducing flooding volume at downstream urban drainage systems. *Sci. Total Environ.* **2020**, *732*, 138931. [CrossRef]

9.　Laio, F.; Porporato, A.; Revelli, R.; Ridolfi, L. A comparison of nonlinear flood forecasting methods. *Water Resour. Res.* **2003**, *39*, 1129. [CrossRef]

10.　Basu, B.; Morrissey, P.; Gill, L.W. Application of Nonlinear Time Series and Machine Learning Algorithms for Forecasting Groundwater Flooding in a Lowland Karst Area. *Water Resour. Res.* **2022**, *58*, e2021WR029576. [CrossRef]

11.　Bafitlhile, T.M.; Li, Z. Applicability of ε-support vector machine and artificial neural network for flood fore-casting in humid, Semi-Humid and Semi-Arid Basins in China. *Water* **2019**, *11*, 85. [CrossRef]

12.　Choubin, B.; Moradi, E.; Golshan, M.; Adamowski, J.; Sajedi-Hosseini, F.; Mosavi, A. An ensemble prediction of flood susceptibility using multivariate discriminant analysis, classification and regression trees, and support vector machines. *Sci. Total Environ.* **2019**, *651*, 2087–2096. [CrossRef] [PubMed]

13.　Dhara, S.; Dang, T.; Parial, K.; Lu, X.X. Accounting for Uncertainty and Reconstruction of Flooding Patterns Based on Multi-Satellite Imagery and Support Vector Machine Technique: A Case Study of Can Tho City, Vietnam. *Water* **2020**, *12*, 1543. [CrossRef]

14.　Basu, B.; Srinivas, V.V. Regional Flood Frequency Analysis Using Entropy-Based Clustering Approach. *J. Hydrol. Eng.* **2016**, *21*, 4016020. [CrossRef]

15.　Duan, H.-F.; Gao, X. Flooding Control and Hydro-Energy Assessment for Urban Stormwater Drainage Systems under Climate Change: Framework Development and Case Study. *Water Resour. Manag.* **2019**, *33*, 3523–3545. [CrossRef]

16.　Varanou, E.; Gkouvatsou, E.; Baltas, E.; Mimikou, M. Quantity and Quality Integrated Catchment Modeling under Climate Change with use of Soil and Water Assessment Tool Model. *J. Hydrol. Eng.* **2002**, *7*, 228–244. [CrossRef]

17.　Githui, F.; Mutua, F.; Bauwens, W. Estimating the impacts of land-cover change on runoff using the soil and water assessment tool (SWAT): Case study of Nzoia catchment, Kenya / Estimation des impacts du changement d'occupation du sol sur l'écoulement à l'aide de SWAT: Étude du cas du bassin de Nzoia, Kenya. *Hydrol. Sci. J.* **2009**, *54*, 899–908. [CrossRef]

18.　Dessu, S.B.; Melesse, A.M. Modelling the rainfall-runoff process of the Mara River basin using the Soil and Water Assessment Tool. *Hydrol. Process.* **2012**, *26*, 4038–4049. [CrossRef]

19.　Gabriel, M.; Knightes, C.; Dennis, R.; Cooter, E. Potential Impact of Clean Air Act Regulations on Nitrogen Fate and Transport in the Neuse River Basin: A Modeling Investigation Using CMAQ and SWAT. *Environ. Model. Assess.* **2014**, *19*, 451–465. [CrossRef]

20.　Volk, M.; Liersch, S.; Schmidt, G. Towards the implementation of the European Water Framework Directive?: Lessons learned from water quality simulations in an agricultural watershed. *Land Use Policy* **2009**, *26*, 580–588. [CrossRef]

21.　Noori, N.; Kalin, L. Coupling SWAT and ANN models for enhanced daily streamflow prediction. *J. Hydrol.* **2016**, *533*, 141–151. [CrossRef]

22.　Madsen, H.; Lawrence, D.; Lang, M.; Martinkova, M.; Kjeldsen, T. Review of trend analysis and climate change projections of extreme precipitation and floods in Europe. *J. Hydrol.* **2014**, *519*, 3634–3650. [CrossRef]

23.　Breugem, A.J.; Wesseling, J.G.; Oostindie, K.; Ritsema, C.J. Meteorological aspects of heavy precipitation in relation to floods–An overview. *Earth Sci. Rev.* **2020**, *204*, 103171. [CrossRef]

24.　Trenberth, K.E. Changes in precipitation with climate change. *Clim. Res.* **2011**, *47*, 123–138. [CrossRef]

25.　Chen, H.; Guo, S.; Xu, C.Y.; Singh, V.P. Historical temporal trends of hydro-climatic variables and runoff response to climate variability and their relevance in water resource management in the Hanjiang basin. *J. Hydrol.* **2007**, *344*, 171–184. [CrossRef]

26.　Morrissey, P.; Nolan, P.; McCormack, T.; Johnston, P.; Naughton, O.; Bhatnagar, S.; Gill, L. Impacts of climate change on groundwater flooding and ecohydrology in lowland karst. *Hydrol. Earth Syst. Sci.* **2021**, *25*, 1923–1941. [CrossRef]

27.　Adhikari, P.; Hong, Y.; Douglas, K.R.; Kirschbaum, D.; Gourley, J.; Adler, R.; Brakenridge, G. A digitized global flood inventory (1998–2008): Compilation and preliminary results. *Nat. Hazards* **2010**, *55*, 405–422. [CrossRef]

28.　Kurnik, B.; van der Linden, P.; Mysiak, J.; Swart, R.J.; Füssel, H.M.; Christiansen, T.; Cavicchia, L.; Gualdi, S.; Mercogliano, P.; Rianna, G.; et al. Weather-and climate-related natural hazards in Europe. In *Climate Change Adaptation and Disaster Risk Reduction in Europe*; No. 15/2017; EEA-European Environment Agency: Copenhagen, Denmark, 2017; pp. 46–91.

29.　Kiely, G. Climate change in Ireland from precipitation and streamflow observations. *Adv. Water Resour.* **1999**, *23*, 141–151. [CrossRef]

30.　Leahy, P.G.; Kiely, G. Short Duration Rainfall Extremes in Ireland: Influence of Climatic Variability. *Water Resour. Manag.* **2011**, *25*, 987–1003. [CrossRef]

31.　Fernando, N.S.; Shrestha, S.; Kc, S.; Mohanasundaram, S. Investigating major causes of extreme floods using global datasets: A case of Nepal, USA & Thailand. *Prog. Disaster Sci.* **2022**, *13*, 100212. [CrossRef]

32.　Tabari, H. Climate change impact on flood and extreme precipitation increases with water availability. *Sci. Rep.* **2020**, *10*, 13768. [CrossRef] [PubMed]

33.　Frei, C.; Schöll, R.; Fukutome, S.; Schmidli, J.; Vidale, P.L. Future change of precipitation extremes in Europe: Intercomparison of scenarios from regional climate models. *J. Geophys. Res. Atmos.* **2006**, *111*, D06105. [CrossRef]

34.　Tierney, J.E.; Poulsen, C.J.; Montañez, I.P.; Bhattacharya, T.; Feng, R.; Ford, H.L.; Hönisch, B.; Inglis, G.N.; Petersen, S.V.; Sagoo, N.; et al. Past climates inform our future. *Science* **2020**, *370*, eaay3701. [CrossRef] [PubMed]

35.　Moncrieff, M.W. Toward a Dynamical Foundation for Organized Convection Parameterization in GCMs. *Geophys. Res. Lett.* **2019**, *46*, 14103–14108. [CrossRef]

36. Li, Z.; Li, Q.; Wang, J.; Feng, Y.; Shao, Q. Impacts of projected climate change on runoff in upper reach of Heihe River basin using climate elasticity method and GCMs. *Sci. Total Environ.* **2020**, *716*, 137072. [CrossRef]

37. Maxino, C.C.; McAvaney, B.J.; Pitman, A.J.; Perkins, S.E. Ranking the AR4 climate models over the Murray-Darling Basin using simulated maximum temperature, minimum temperature and precipitation. *Int. J. Climatol. A J. R. Meteorol. Soc.* **2008**, *28*, 1097–1112. [CrossRef]

38. Mujumdar, P.P.; Kumar, D.N. *Floods in A Changing Climate: Hydrologic Modeling*; Cambridge University Press: Cambridge, UK, 2012.

39. Parker, D.; Folland, C.; Scaife, A.; Knight, J.; Colman, A.; Baines, P.; Dong, B. Decadal to multidecadal variability and the climate change background. *J. Geophys. Res. Atmos.* **2007**, *112*, D18115. [CrossRef]

40. Felder, G.; Gómez-Navarro, J.J.; Zischg, A.P.; Raible, C.C.; Röthlisberger, V.; Bozhinova, D.; Martius, O.; Weingartner, R. From global circulation to local flood loss: Coupling models across the scales. *Sci. Total Environ.* **2018**, *635*, 1225–1239. [CrossRef]

41. Hewitson, B.; Crane, R. Climate downscaling: Techniques and application. *Clim. Res.* **1996**, *7*, 85–95. [CrossRef]

42. Rummukainen, M. State-of-the-art with regional climate models. *Wiley Interdiscip. Rev. Clim. Change* **2010**, *1*, 82–96. [CrossRef]

43. Rana, A.; Foster, K.; Bosshard, T.; Olsson, J.; Bengtsson, L. Impact of climate change on rainfall over Mumbai using Distribution-based Scaling of Global Climate Model projections. *J. Hydrol. Reg. Stud.* **2014**, *1*, 107–128. [CrossRef]

44. Rana, A.; Moradkhani, H.; Qin, Y. Understanding the joint behavior of temperature and precipitation for climate change impact studies. *Theor. Appl. Climatol.* **2017**, *129*, 321–339. [CrossRef]

45. Wood, A.; Leung, L.R.; Sridhar, V.; Lettenmaier, D.P. Hydrologic Implications of Dynamical and Statistical Approaches to Downscaling Climate Model Outputs. *Clim. Chang.* **2004**, *62*, 189–216. [CrossRef]

46. Boé, J.; Terray, L.; Habets, F.; Martin, E. Statistical and dynamical downscaling of the Seine basin climate for hydro-meteorological studies. *Int. J. Clim. J. R. Meteorol. Soc.* **2007**, *27*, 1643–1655. [CrossRef]

47. Mejia, J.F.; Huntington, J.; Hatchett, B.; Koracin, D.; Niswonger, R.G. Linking global climate models to an integrated hydrologic model: Using an individual station downscaling approach. *J. Contemp. Water Res. Educ.* **2012**, *147*, 17–27. [CrossRef]

48. Salvi, K.; Ghosh, S.; Ganguly, A.R. Credibility of statistical downscaling under nonstationary climate. *Clim. Dyn.* **2016**, *46*, 1991–2023. [CrossRef]

49. Kannan, S.; Ghosh, S. A nonparametric kernel regression model for downscaling multisite daily precipitation in the Mahanadi basin. *Water Resour. Res.* **2013**, *49*, 1360–1385. [CrossRef]

50. Fowler, H.J.; Blenkinsop, S.; Tebaldi, C. Linking climate change modelling to impacts studies: Recent advances in downscaling techniques for hydrological modelling. *Int. J. Clim. A J. R. Me-Teorological Soc.* **2007**, *27*, 1547–1578. [CrossRef]

51. Teutschbein, C.; Wetterhall, F.; Seibert, J. Evaluation of different downscaling techniques for hydrological cli-mate-change impact studies at the catchment scale. *Clim. Dyn.* **2011**, *37*, 2087–2105. [CrossRef]

52. Huth, R. Statistical downscaling in central Europe: Evaluation of methods and potential predictors. *Clim. Res.* **1999**, *13*, 91–101. [CrossRef]

53. Fatichi, S.; Ivanov, V.Y.; Caporali, E. Assessment of a stochastic downscaling methodology in generating an ensemble of hourly future climate time series. *Clim. Dyn.* **2013**, *40*, 1841–1861. [CrossRef]

54. Villarini, G.; Smith, J.A.; Serinaldi, F.; Bales, J.; Bates, P.D.; Krajewski, W.F. Flood frequency analysis for non-stationary annual peak records in an urban drainage basin. *Adv. Water Resour.* **2009**, *32*, 1255–1266. [CrossRef]

55. Pilla, F.; Gharbia, S.S.; Lyons, R. How do households perceive flood-risk? The impact of flooding on the cost of accommodation in Dublin, Ireland. *Sci. Total Environ.* **2019**, *650*, 144–154. [CrossRef] [PubMed]

56. Arnold, J.G.; Allen, P.M.; Bernhardt, G. A comprehensive surface-groundwater flow model. *J. Hydrol.* **1993**, *142*, 47–69. [CrossRef]

57. Arnold, J.G.; Srinivasan, R.; Muttiah, R.S.; Williams, J.R. Large area hydrologic modeling and assessment part I: Model development. *JAWRA J. Am. Water Resour. Assoc.* **1998**, *34*, 73–89. [CrossRef]

58. Arnold, J.G.; Muttiah, R.S.; Srinivasan, R.; Allen, P.M. Regional estimation of base flow and groundwater re-charge in the Upper Mississippi river basin. *J. Hydrol.* **2000**, *227*, 21–40. [CrossRef]

59. Allen, R.G.; Pereira, L.S.; Raes, D.; Smith, M. *Crop Evapotranspiration-Guidelines for Computing Crop Water Requirements—FAO Irrigation and Drainage Paper 56*; FAO: Rome, Italy, 1998; Volume 300, p. D05109.

60. Srinivasan, R.; Arnold, J.G.; Jones, C.A. Hydrologic modelling of the United States with the soil and water assessment tool. *Int. J. Water Resour. Dev.* **1998**, *14*, 315–325. [CrossRef]

61. Cibin, R.; Sudheer, K.P.; Chaubey, I. Sensitivity and identifiability of stream flow generation parameters of the SWAT model. *Hydrol. Process. Int. J.* **2010**, *24*, 1133–1148. [CrossRef]

62. Abbaspour, K.C.; Yang, J.; Maximov, I.; Siber, R.; Bogner, K.; Mieleitner, J.; Zobrist, J.; Srinivasan, R. Model-ling hydrology and water quality in the pre-alpine/alpine Thur watershed using SWAT. *J. Hydrol.* **2007**, *333*, 413–430. [CrossRef]

63. Abbaspour, K.C. Swat-Cup 2012. SWAT Calibration and Uncertainty Program—A User Manual. 2013. Available online: https://sndl.ucmerced.edu/files/San_Joaquin/Model_Work/SWAT_MercedRiver/SWATCUP/Usermanual_Swat_Cup_2012.pdf (accessed on 1 March 2022).

64. Ghosh, S.; Mujumdar, P. Statistical downscaling of GCM simulations to streamflow using relevance vector machine. *Adv. Water Resour.* **2008**, *31*, 132–146. [CrossRef]

65. Li, H.; Sheffield, J.; Wood, E.F. Bias correction of monthly precipitation and temperature fields from Intergovernmental Panel on Climate Change AR4 models using equidistant quantile matching. *J. Geophys. Res. Atmos.* **2010**, *115*, D10101. [CrossRef]

66. Te Chow, V. *Applied Hydrology*; Tata McGraw-Hill Education: New York, NY, USA, 2010.

67. Coles, S. *An Introduction to Statistical Modeling of Extreme Values*; Springer: London, UK, 2001; Volume 208, p. 208.

68. Brunner, G.W. HEC-RAS River Analysis System. In *Hydraulic Reference Manual. Version 1.0*; Army Corps of Engineers, Hydrologic Engineering Center: Davis, CA, USA, 1995.

69. Lamichhane, N.; Sharma, S. Effect of input data in hydraulic modeling for flood warning systems. *Hydrol. Sci. J.* **2018**, *63*, 938–956. [CrossRef]

70. Horritt, M.; Bates, P. Evaluation of 1D and 2D numerical models for predicting river flood inundation. *J. Hydrol.* **2002**, *268*, 87–99. [CrossRef]

71. Alho, P.; Aaltonen, J. Comparing a 1D hydraulic model with a 2D hydraulic model for the simulation of extreme glacial outburst floods. *Hydrol. Processes: Int. J.* **2008**, *22*, 1537–1547. [CrossRef]

72. Cook, A.; Merwade, V. Effect of topographic data, geometric configuration and modeling approach on flood inundation mapping. *J. Hydrol.* **2009**, *377*, 131–142. [CrossRef]

73. Costabile, P.; Macchione, F.; Natale, L.; Petaccia, G. Flood mapping using LIDAR DEM. Limitations of the 1-D modeling highlighted by the 2-D approach. *Nat. Hazards* **2015**, *77*, 181–204. [CrossRef]

74. Brunner, G.W. *HEC-RAS River Analysis System User's Manual. Version 6.0*; Army Corps of Engineers, Hydrologic Engineering Center: Davis, CA, USA, 2021.

75. GRAS, D. *EU-DEM Statistical Validation Report*; European Environment Agency: Copenhagen, Denmark, 2014.

76. Basu, B. Development of soil and land cover databases for use in the Soil Water Assessment Tool from Irish National Soil Maps and CORINE Land Cover Maps for Ireland. *Earth Syst. Sci. Data Discuss* **2021**, *in press*. [CrossRef]

77. Cordeiro, M.R.; Lelyk, G.; Kröbel, R.; Legesse, G.; Faramarzi, M.; Masud, M.B.; McAllister, T. Deriving a dataset for agriculturally relevant soils from the Soil Landscapes of Canada (SLC) database for use in Soil and Water Assessment Tool (SWAT) simulations. *Earth Syst. Sci. Data* **2018**, *10*, 1673–1686. [CrossRef]

78. Basu, B. Soil, Landcover and DEM Database for Ireland to be Used with SWAT Model. ZENODO. 2021. Available online: https://zenodo.org/record/4767926#.YlUdIdNByUk (accessed on 1 March 2022).

79. Fealy, R.; Bruyére, C.; Duffy, C. *Regional Climate Model Simulations for Ireland for the 21st Century*; Environmental Protection Agency: Johnstown Castle, Ireland, 2018; pp. 264–268.

80. Stocker, T.F.; Qin, D.; Plattner, G.K.; Alexander, L.V.; Allen, S.K.; Bindoff, N.L.; Bréon, F.M.; Church, J.A.; Cubasch, U.; Emori, S.; et al. Technical summary. In *Climate Change 2013: The Physical Science Basis*; Contribution of Working Group I to the Fifth Assessment Report of the Intergovernmental Panel on Climate Change; Cambridge University Press: Cambridge, UK, 2013; pp. 33–115.

81. Basu, A.S.; Gill, L.W.; Pilla, F.; Basu, B. Assessment of Variations in Runoff Due to Landcover Changes Using the SWAT Model in an Urban River in Dublin, Ireland. *Sustainability* **2022**, *14*, 534. [CrossRef]